Laser-Driven Planar Rayleigh-Taylor Instability Experiments

S. G. Glendinning, S. V. Weber, P. Bell, L. B. DaSilva, S. N. Dixit, M. A. Henesian, D. R. Kania, J. D. Kilkenny, H. T. Powell, R. J. Wallace, and P. J. Wegner
Lawrence Livermore National Laboratory, University of California, Livermore, California 94550

J. P. Knauer and C. P. Verdon
Laboratory for Laser Energetics, University of Rochester, Rochester, New York 14623
(Received 6 April 1992)

We have performed a series of experiments on the Nova Laser Facility to examine the hydrodynamic behavior of directly driven planar foils with initial perturbations of varying wavelength. The foils were accelerated with a single, frequency doubled, smoothed and temporally shaped laser beam at 0.8×10^{14} W/cm^2. The experiments are in good agreement with numerical simulations using the computer codes LASNEX and ORCHID which show growth rates reduced to about 70% of classical for this nonlinear regime.

PACS numbers: 52.35.Py, 52.65.+z, 52.70.−m

Hydrodynamic instabilities during directly driven implosions of inertially confined fusion capsules are expected to play a dominant role in determining overall capsule performance [1–3]. Therefore, understanding the development of the Rayleigh-Taylor instability at conditions as close as possible to those predicted for high gain, directly driven capsule designs using currently available laser systems is an important step in furthering our understanding of the potential importance of such instabilities. Indirectly driven experiments, that is, experiments in which the drive is provided by laser light converted to soft x rays [4], have shown good agreement between measurements and calculations. However, experiments extending back over several years [5–7] in which the sample is directly driven by a laser have not; nearly all previous reports measured growth rates less than predicted. We demonstrate here for the first time agreement between measured Rayleigh-Taylor growth and detailed calculations from two computer codes, LASNEX [8] at LLNL and ORCHID at LLE. The two simulations each showed quantitative agreement with the experimental results obtained during this series of experiments. For brevity in this paper we will limit the presentation of simulation results to those from LASNEX. Our experimental conditions are shown in Table I.

In order to generate a smooth, nearly flat-topped laser intensity distribution at 0.53 μm we have added three smoothing components to one beam of Nova: a random phase plate (RPP) [9,10], steering wedges, and spectral dispersion (SSD) [11,12]. The RPP produces a speckle pattern (speckle size ~6 μm) with an envelope which is the diffraction pattern from a hexagonal aperture, with a zero to zero diameter of 1000 μm. This distribution has two disadvantages for this experiment: First, the distribution of speckle magnitudes gives rise to a large nonuniformity (normalized standard deviation of 100% [13]) at high spatial frequencies which could interfere with an attempt to measure the growth of surface perturbations seeded at similar frequencies. Second, the sharply peaked envelope will drive the edges of a 700-μm-diam foil with only about half the intensity as at the center, making the experimental conditions far from planar. Therefore, the beam was split into nine segments, each independently steered in space with a glass wedge to form a flat-topped intensity distribution. We used the technique of SSD to smooth short scale length nonuniformities. For our implementation, the 1.053-μm laser pulse was cross-phase-modulated in an optical fiber with a pulse from a noisy ($\delta\nu\sim450$ GHz) oscillator. The resultant pulse had $\delta\nu/\nu=0.14\%$ FWHM; this broadband pulse was dispersed by a diffraction grating. The measured time integrated smoothed beam intensity distribution is shown in Fig. 1. This distribution has a normalized standard deviation of 8% over a 700-μm diameter.

TABLE I. Experimental conditions.

Intensity (peak) (W/cm^2)	0.8×10^{14}
Laser wavelength (μm)	0.53
Acceleration (cm/s^2)	0.6×10^{16}
Hydrodynamic growth	exp(3)
Perturbation wavelengths (μm)	20,30,50,70
Initial amplitudes (μm)	1

The drive pulse shape for these experiments was nominally a linear 1-ns ramp followed by a 2-ns flat section at $\sim0.8\times10^{14}$ W/cm^2, a shape chosen to reduce the initial shock driving the foil while providing nearly constant acceleration. The backlighter laser pulse was nominally a 3-ns square pulse at 8×10^{14} W/cm^2. The incident power was measured by calorimetry and by optical streak-camera profiles; the intensity was estimated from the relative energy distribution shown in Fig. 1. The large laser spot has considerable energy present at lower intensities, making a direct energy balance measurement of absorption difficult; instead we inferred the absorbed intensity from measurements of the shock transit time in thicknesses between 30 and 90 μm of plastic, using a streak camera coupled to an optical imager filtered at 420

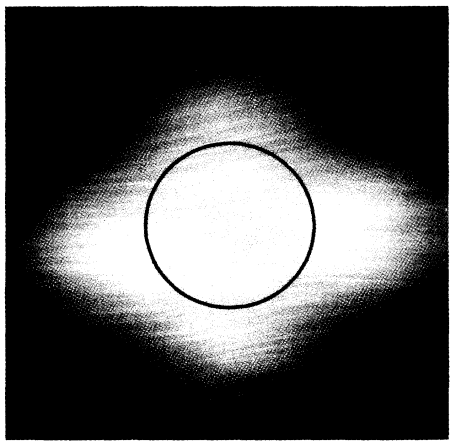

FIG. 1. Logarithm of the far-field exposure distribution of the drive laser beam, converted from film density. The FWHM across the center is 1500 μm; the circle represents the 700-μm target used for these experiments. The fine horizontal streaks are characteristic of SSD.

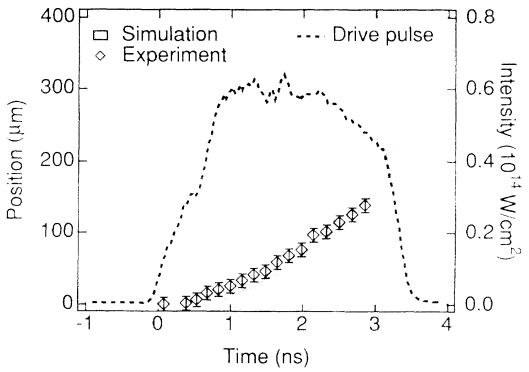

FIG. 2. Target position (diamonds) as a function of time. Calculated position is shown as a shaded curve whose width is due to the uncertainty in drive. The drive laser pulse shape in W/cm^2 is also shown (dashed curve).

nm. The LASNEX predictions agree with the shock transit times within the experimental errors (100 ps), from which we infer an absorption fraction of $(100 \pm 13)\%$ (10% due to timing uncertainties, 9% due to errors in the incident intensity). This is slightly higher than previous measurements of absorption with unsmoothed beams (80%) [14]. The shock velocities vary between 24 and 34 μm/ns, giving pressures between 6 and 12 Mbar, depending on the plastic thickness.

To establish the acceleration of the foils we have also measured the trajectory of a driven foil, using a streaked x-ray pinhole camera to radiograph an unmodulated foil viewed edge on, backlit by x rays produced by a gold disk. An example of the experimental and simulated results is shown in Fig. 2 along with the drive pulse. The acceleration was nearly constant at 50 μm/ns^2 after the shock breaks out at $t = 0.7$ ns (giving an inferred drive pressure of 9 Mbar during the acceleration phase, consistent with the shock measurements). The resultant trajectory agrees with the LASNEX predictions, using the 100% absorption described above.

The primary diagnostic for the face-on experiment is a gated x-ray pinhole camera, used to view a backlit driven foil as shown in Fig. 3. The backlighting beam is incident from one side, and the drive (smoothed) beam is incident from the other side onto a target which normally has preformed modulations; the target normal is parallel to the drive beam and the modulations are toward the beam. X rays from the backlighter target (uranium) are filtered with 12 μm Be before reaching the driven foil to eliminate x-ray preheat from the backlighter. Because the two beams are opposed, it is not possible to view the driven foil exactly face on. The angle between the line of sight of the pinhole camera and the motion of the foil is 16°.

The foils were made of polyethylene (density of 1.0 g/cm^3), typically 800 μm in diameter and 18–22 μm thick. These foils had sinusoidal modulations impressed on one side by a micromachined mold; the thickness and modulation depth were measured to $\pm 10\%$ by contact profilometry. The foils were coated on both sides with 0.08 μm Al to prevent shine-through of laser light [15]. They were then mounted on the back side (i.e., side away from the drive beam) of a Mylar washer 100 μm thick and 3 mm in diameter with a 700-μm hole. (The targets for the side-on experiments were identical except they were not modulated and used a gold backlighter mounted to one side of the foil.)

The gated pinhole camera is an array of four strips of fast gated microchannel plate (MCP) detectors [16] on a single 40-mm-diam microchannel plate. The radiographed foil is imaged by an array of 10-μm-diam pinholes onto four strips, thus providing multiple images at different times with 100-ps time resolution. The time between strip gates was typically 800 ps, while the time between frames on a single strip was 76 ps. The spatial

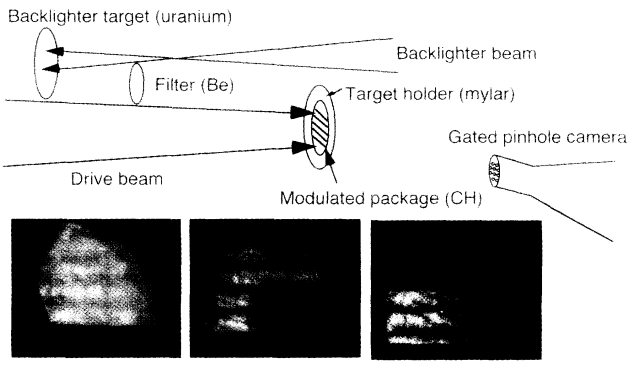

FIG. 3. Experimental configuration and three frames from 70-μm wavelength, 1-μm initial amplitude experimental data, shown in ln(exposure). The frame times are $t_0 + 1.2$, $t_0 + 2.0$, and $t_0 + 2.8$, ± 100 ps.

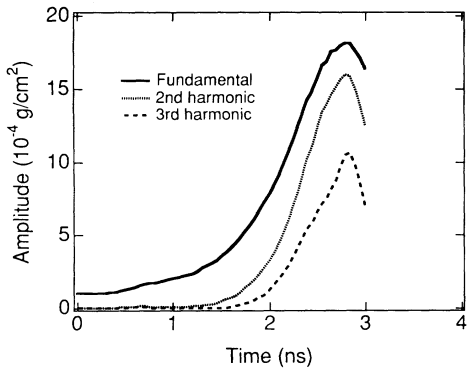

FIG. 4. LASNEX simulation of growth in column density for a 1-μm initial amplitude, 70-μm wavelength perturbation.

resolution as expressed by the modulation transfer function (MTF) or point spread function (PSF) for this diagnostic is an essential part of these experiments. We measured backlit grids to determine the PSF of the combination of the pinhole camera and the gated MCP, and found that the PSF was approximately Gaussian with a full width at half maximum of 8 μm.

In order to verify that the current beam smoothing techniques are sufficient for the experiments, we have tested the effect of our drive beam structure by driving nominally flat foils in the same configuration as our modulated foils. The structure of fine horizontal lines visible in the beam profile (Fig. 1) is also visible in the experimental radiographs at about 2.1 ns after the start of the drive; separate gated pinhole camera images of the backlighter show that the structure is not due to the backlighter. One-dimensional Fourier decompositions (perpendicular to the SSD dispersion direction) of a portion of the radiograph where the modulation is greatest indicate that the modulation is about 20% of that due to the imposed perturbations, about the same as the measured scatter in the data. Because the phase of this modulation is random with respect to the imposed surface perturbations, it is likely that the modulation due to the beam accounts for the observed scatter of the data.

The main goal of these experiments was the measurement of wavelength scaling of Rayleigh-Taylor growth of initially seeded single wavelength surface perturbations. We have measured four wavelengths, $\lambda = 20$, 30, 50, and 70 μm, with an initial modulation amplitude of 1 μm (2 μm peak to valley). A typical set of images obtained from the gated pinhole camera is shown in Fig. 3. This shot used a $\lambda = 70$ μm target; the times for the three strips are $t_0 + 1.2$ ns, $t_0 + 2.0$ ns, and $t_0 + 2.8$ ns. In order to convert the data to a set of amplitudes comparable to post-processed LASNEX results, we reduced each digitized image to a vertical cross section and averaged in the horizontal direction, taking care to avoid regions where the exposure is so low that the instrument dynamic range is insufficient. The averaged cross sections still show long scale length structure characteristic of the backlighter spot; this structure is removed by fitting a smoothly varying background. The optical depth is then calculated as the natural logarithm of the cross section divided by the smoothed background.

Figure 4 shows the calculated growth of perturbations in column density $\Delta\rho z$ for a typical case, where $\lambda = 70$ μm. The amplitude of the perturbation is described by the Fourier coefficients of the harmonic modes in column density through the sample. The first 1.2 ns of the growth shows transient effects due to the rise of the drive and shock passage through the sample. Then about two e-foldings of nearly exponential (but weakly nonlinear, as evinced by the presence of higher harmonics) growth are seen before the perturbations saturate at amplitudes comparable to the original foil column density. Since x-ray transmission is measured, not the column density, we then simulated the attenuation of the measured backlighter spectrum through the sample, convolved the resulting exposure with the instrumental PSF, and took the natural logarithm to compare amplitude in optical depth with experimental data. The Fourier decomposition of the processed data was then compared with the LASNEX simulations (Fig. 5). Each period was analyzed separately and the error bars shown in Fig. 5 are the standard deviation of the set of periods.

No systematic discrepancy is apparent in the comparison of the data with the LASNEX simulations; in particu-

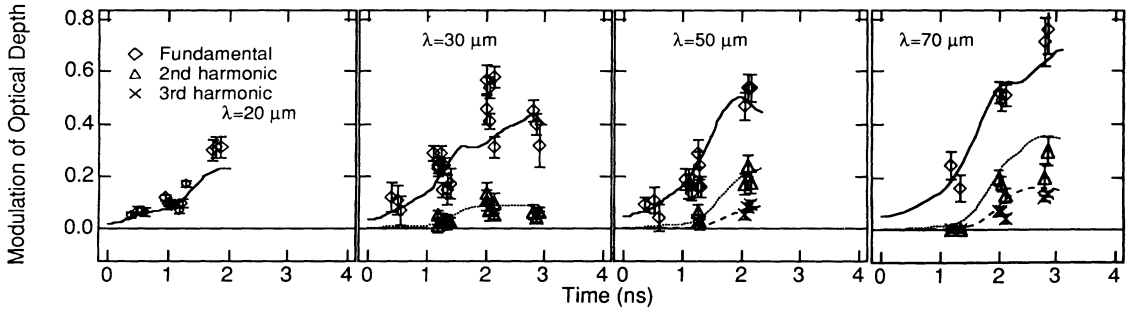

FIG. 5. Comparison of experimental data with LASNEX simulations. The fundamental (solid curve), second-harmonic (dotted curve), and third-harmonic (dashed curve) simulations are shown vs time.

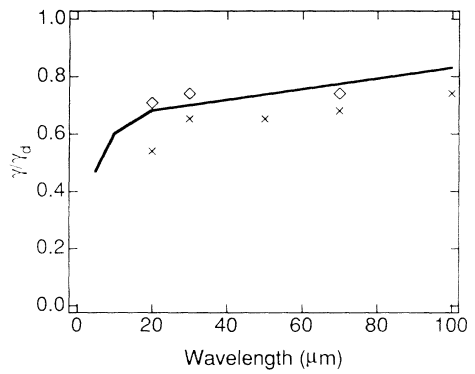

FIG. 6. Comparison of simulated growth rates normalized to classical for linear and nonlinear regimes. Crosses are simulations for these experimental conditions, and diamonds are for the same drive conditions but initial amplitude of 0.1 μm (linear). The solid line is the expression of Ref. [17].

lar, the low growth at various wavelengths [5–7] seen by earlier researchers is not observed in our experiment. Because the present experiments have almost none of the growth in a purely linear Rayleigh-Taylor region, comparison of the growth rates to classical or ablatively stabilized classical growth rates [17] must be done with care. We have performed simulations in the linear ($a_0=0.1$ μm) regime and show in Fig. 6 growth rates from those simulations, from simulations of the current experiments, and ablatively stabilized classical growth, all normalized to classical values. Note that the fits to the simulations were made to the exponential growth phase only, eliminating intervals of transient structure ($t < 1.2$ ns) and saturation. We use the expression of Ref. [17] [$\gamma = 0.9(kg)^{1/2} - 3kV_a$, where k is the wave number , g is the acceleration, and V_a is the ablation velocity (~ 1 μm/ns for our experiment based on numerical simulations)]. It may be seen that this expression describes our modeling in the linear region rather well; the growth rates for experiments in the nonlinear region are reduced to about 85% of this, lower at shorter wavelengths.

In summary, we have observed the Rayleigh-Taylor unstable hydrodynamic development of planar foils at several initially imposed wavelengths driven by a spatially smoothed, temporally shaped Nova laser beam. We found that measured and simulated foil trajectory and shock transit times were in good agreement. In addition, we found that the measured development of the observed harmonics was in good agreement with the numerical simulations at all wavelengths, in contrast with previous experimental results reported in the literature. Our simulations indicate a reduction of the growth rate in the linear region to about 0.7–0.8 of classical at these wavelengths.

These results represent an initial series of experiments in which the observed modulations quickly become nonlinear and in which no attempt was made to choose experimental conditions which could reduce the growth of the Rayleigh-Taylor instability. Future experiments will investigate Rayleigh-Taylor growth in the linear region and the increase of stabilization by various means.

We wish to acknowledge D. Browning, R. Kauffman, H. Kornblum, I. Thomas, T. Weiland, J. Wiedwald, R. Wilcox, and B. Woods for their significant contributions to these experiments, M. Prasad for enhancements to LASNEX, and the Nova laser staff for their expert and dedicated operation. This work was performed under the auspices of the U.S. DOE by the Lawrence Livermore National Laboratory under Contract No. W-7405-ENG-48.

[1] J. Nuckolls *et al.*, Nature (London) **239**, 139 (1972).
[2] S. Bodner, Phys. Rev. Lett. **33**, 761 (1974).
[3] J. D. Lindl and W. C. Meade, Phys. Rev. Lett. **34**, 1273 (1975).
[4] B. Remington *et al.*, Phys. Rev. Lett. **67**, 3259 (1991); J. D. Kilkenny, Phys. Fluids B **2**, 1400 (1990).
[5] A. J. Cole *et al.*, Nature (London) **299**, 329 (1982).
[6] J. Grun *et al.*, Phys. Rev. Lett. **58**, 2672 (1987).
[7] M. Desselberger *et al.*, Phys. Rev. Lett. **65**, 2997 (1990).
[8] G. B. Zimmerman and W. L. Kruer, Comments Plasma Phys. Controlled Fusion **2**, 51 (1975).
[9] X. Deng *et al.*, Appl. Opt. **25**, 377 (1986).
[10] Y. Kato *et al.*, Phys. Rev. Lett. **53**, 1057 (1984).
[11] S. Skupsky *et al.*, J. Appl. Phys. **66**, 3456 (1989).
[12] H. Powell, S. N. Dixit, M. A. Henesian, *ICF Quarterly Report* (Report No. UCRL-LR-105821-91-1, 1991, Vol. 1, p. 28.
[13] J. W. Goodman, in *Laser Speckle and Related Phenomena*, edited by J. C. Dainty (Springer, Berlin, 1984), Chap. 2.
[14] C. Garban-Labaune *et al.*, Phys. Fluids **28**, 2580 (1985).
[15] J. Delletrez *et al.*, "Effect of Barrier Layers in Burn-Through Experiments with 351-nm Laser Illumination," Lab Report No. 208, URLLE 1990 (to be published).
[16] J. D. Kilkenny, Laser Part. Beams **9**, 49 (1991).
[17] H. Takabe, L. Montierth, and R. L. Morse, Phys. Fluids **26**, 2299 (1983); H. Takabe *et al.*, *ibid.* **28**, 3676 (1985).

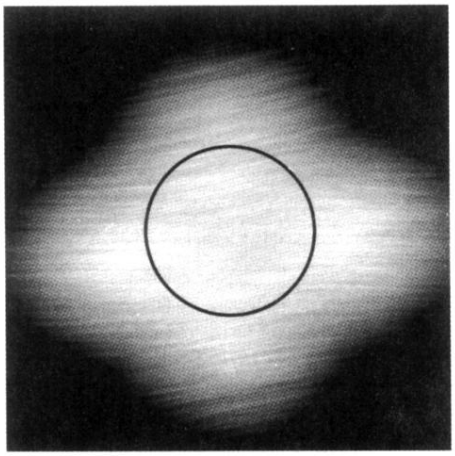

FIG. 1. Logarithm of the far-field exposure distribution of the drive laser beam, converted from film density. The FWHM across the center is 1500 μm; the circle represents the 700-μm target used for these experiments. The fine horizontal streaks are characteristic of SSD.

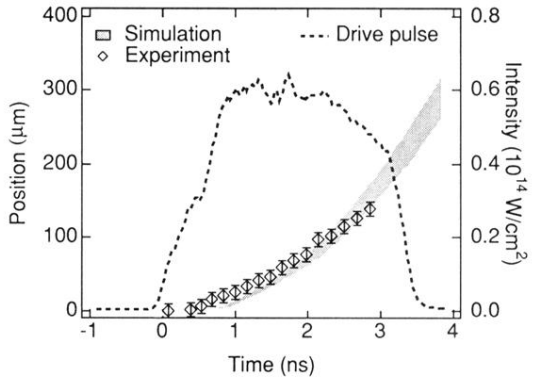

FIG. 2. Target position (diamonds) as a function of time. Calculated position is shown as a shaded curve whose width is due to the uncertainty in drive. The drive laser pulse shape in W/cm^2 is also shown (dashed curve).

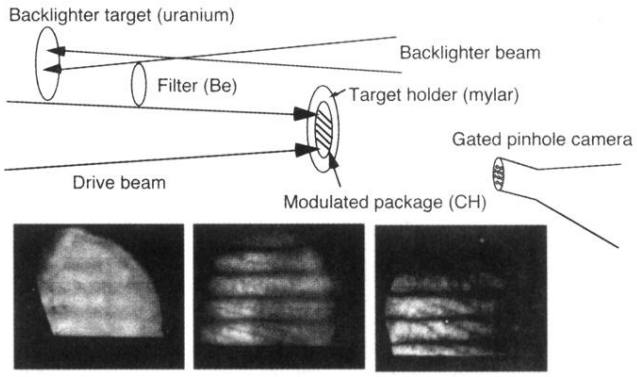

FIG. 3. Experimental configuration and three frames from 70-μm wavelength, 1-μm initial amplitude experimental data, shown in ln(exposure). The frame times are $t_0+1.2$, $t_0+2.0$, and $t_0+2.8$, $\pm$ 100 ps.